Fast Iterative Schemes for the Solution of Eddy-Current Problems Featuring Multiple Conductors by Integral Formulations

Mauro Passarotto[1], Ruben Specogna[1], and Christophe Geuzaine[2]

[1]EMC Laboratory, Polytechnic Department of Engineering and Architecture (DPIA), Università di Udine, 33100 Udine, Italy
[2]Institut Montefiore B28, ACE, Université de Liège, 4000 Liège, Belgium

Integral formulations lead to full matrices that, despite the use of efficient low-rank approximation techniques, are impossible to be solved when the number of unknowns is large enough. To overcome this limitation, we propose a novel direct-iterative hybrid technique to solve eddy currents by taking advantage of the domain splitting into disjoint conductors: each subproblem is solved via direct solvers on each subdomain, whereas the Krylov subspace techniques are applied to compute the mutual effects between the substructures iteratively. In this way, the entries related to the mutual contributions between the subdomains are not stored. In particular, this article focuses on testing the convergence of the iterative method.

Index Terms—**Eddy currents, integral formulations, iterative methods, Krylov subspace, subdomains, substructuring.**

I. Introduction

MATRIX-COMPRESSION techniques based on low-rank approximations [1] are the major contributors to the renewed interest in integral formulations for the numerical solution of eddy-current problems [2]–[5]. These techniques exploit the matrix structure of the overall problem in order to reduce the number of entries of the otherwise fully populated system matrix.

A different approach to reach the goal of avoiding the computation and storage of full matrices of the whole problem is represented by iterative techniques, which may be combined with matrix compression to reduce the problem size further. Focusing on the eddy-current problems, in [6], some of the authors have already presented an iterative formulation inspired by that in [7] to solve the eddy-current problems in the frequency domain with the volumetric integral formulation from [5]. In that case, only the entries of a sparse system have to be computed and stored, leading to a Jacobi iterative algorithm whose convergence was shown to be quite slow for general eddy-current problems.

In this article, a novel direct-iterative hybrid technique for eddy currents, inspired by the method described in [8] for multiple-scattering problems, is proposed: on the one hand, the overall domain is split into several disconnected subdomains, each of them is then solved as an independent problem by a direct solver, thus reducing the size of the system to be stored; on the other hand, an improved iterative scheme is developed to compute the mutual effects between the subdomains to ensure the scheme convergence and to minimize the number of iterations. To pursue this last goal, the Gauss–Seidel (GS) scheme is compared with more sophisticated iterative techniques based on the Krylov subspaces in order to study the convergence; in relation to this, it is shown that, for this formulation, the best method to achieve robustness and fast convergence is the generalized minimum residual (GMRES) method [9].

The remaining part of this article is organized as follows: in Section II, the details of this new iterative scheme applied to the volume integral formulation of [5] are reported. To write the equations, we use the geometric framework, whose details can be found in [5], but, thanks to [10], this is one of the cases in which the solution is the same as the equivalent finite-element integral method on the tetrahedral meshes [3]. The advantage of this geometric formulation is that it can be used on general polygonal/polyhedral elements. In Section III, we then outline the most common methods based on the Krylov subspace theory and we compare their performance. Finally, Section IV draws the conclusions.

II. Iterative Scheme

In this section, the main equations of the proposed direct-iterative hybrid method are reported. For the sake of simplicity, we will here refer to a simply-connected conducting domain Ω_c, but the same approach can be easily extended to topologically non-trivial domains too, following the same reasoning in [5].

An eddy-current problem in the frequency domain written on the geometrical framework shown in Fig. 1, by means of the volume integral formulation whose details can be found in [5], leads to a system of equations that reads as

$$\mathbf{KT} = \mathbf{b}_s. \tag{1}$$

The system matrix $\mathbf{K}$ can be partitioned as $\mathbf{K} = \mathbf{K}_R + j\omega\mathbf{K}_M$ with $\mathbf{K}_R$ a sparse matrix, $\mathbf{K}_M$ a fully populated one, and ω the angular frequency. The right-hand side vector $\mathbf{b}_s$ is constituted by the terms that are proportional to the circulation of the magnetic vector potential A_s generated by a given

Manuscript received August 6, 2019; revised October 15, 2019; accepted November 11, 2019. Date of publication January 14, 2020; date of current version February 19, 2020. Corresponding author: M. Passarotto (e-mail: passarotto.mauro@spes.uniud.it).

Color versions of one or more of the figures in this article are available online at http://ieeexplore.ieee.org.

Digital Object Identifier 10.1109/TMAG.2019.2954071

0018-9464 © 2020 IEEE. Personal use is permitted, but republication/redistribution requires IEEE permission.
See https://www.ieee.org/publications/rights/index.html for more information.

Authorized licensed use limited to: University of Udine. Downloaded on January 25,2021 at 10:42:39 UTC from IEEE Xplore. Restrictions apply.

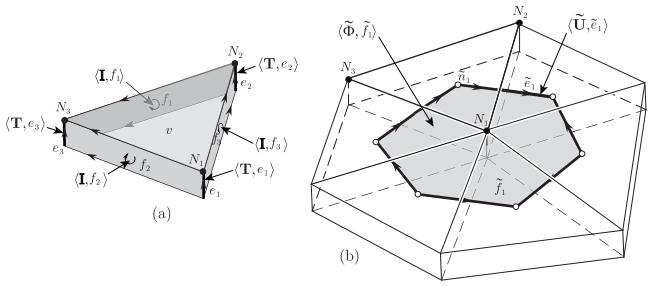

Fig. 1. Geometrical elements and association with the physical variable of the considered eddy-current formulation for (a) volume v of the *primal grid* and (b) *dual grid* [11].

source of magnetic field (e.g., a coil). Finally, the vector of the degrees of freedom (DOFs) $\mathbf{T}$ stores the integral of the electric vector potential along the primal grid edges.

Given $\Omega_i, i \in \{1, 2, \ldots, N\}$ distinct subdomains, partitioning the whole geometry Ω_c such that $\Omega_c = \Omega_1 \cup \Omega_2 \cup \ldots \cup \Omega_N$, a block-diagonal matrix $\mathbf{K}_{SD}$ can be defined as

$$\mathbf{K}_{SD} = \begin{bmatrix} \mathbf{K}_1 & \mathbf{0} & \cdots & \mathbf{0} \\ \mathbf{0} & \mathbf{K}_2 & \cdots & \mathbf{0} \\ \vdots & \vdots & \ddots & \vdots \\ \mathbf{0} & \mathbf{0} & \cdots & \mathbf{K}_N \end{bmatrix} \tag{2}$$

where each $\mathbf{K}_i = \mathbf{K}_{R_i} + j\omega\mathbf{K}_{M_i}$ is related and limited to the only subdomain Ω_i. Similarly, also the vector $\mathbf{T}$ can be partitioned accordingly to the subdomains as $\mathbf{T} = \left[\mathbf{T}_1^T\ \mathbf{T}_2^T\ \cdots\ \mathbf{T}_N^T\right]^T$.

In order to recover (1), the missing mutual terms linking two different distinct subdomains have to be expressed. Similar to what was done in [12], starting from the current density flowing in each subdomain, we can express the coupling between two of them by calculating the magnetic vector potential $\vec{A}(r)$ generated on an arbitrary point of the space r by a constant current density $\vec{J}_v$ in a volume v of the grid thanks to [13]. However, we remark that differently to [12], we do not compute equivalent currents on an additional coupling surface (thus approximating the original problem), but we propose a new iterative formulation that equivalently solves the initial system of equations.

Referring to [13], we define $P_{g,v}(r) := \sum_{S_f \in \partial v}(r_f - r) \cdot n_f W_f(r)$ as a scalar geometrical parameter that depends only on the geometry of v and on r, with r_f a point on the face f of v and n_f a unit normal vector of this face. $W_f(r)$ is another geometrical parameter that the reader can find in [13]. Then, we can expand the current density term, using the relations in [5], leading to

$$\vec{A}(r) = \frac{\mu_0 P_{g,v}(r)}{8\pi\,|v|} \cdot \sum_{k=1}^{F} I^k \tilde{e}^k \tag{3}$$

with $|v|$ the volume of v, F its total number of faces, I^k the current flowing through the kth face, and $\tilde{e}^k$ the kth dual edge of the dual grid. Dual edges are in a one-to-one correspondence with the primal grid faces, as it can be deduced from Fig. 1.

Successively, defining $\mathbf{C}_{ih}$ as the face-edge incidence matrix of the subdomains Ω_i and Ω_h, since the flux $\tilde{\Phi}_i$ of the magnetic field across the dual faces $\tilde{f}$ of Ω_i, generated by the currents $\mathbf{I}_h$ flowing in Ω_h, can be written in terms of a magnetic constitutive matrix $\mathbf{M}_{ih}^{\Delta}$ as

$$\tilde{\Phi}_i = \mathbf{C}_{ih}^T \mathbf{M}_{ih}^{\Delta} \mathbf{I}_h = \mathbf{C}_{ih}^T \mathbf{M}_{ih}^{\Delta} \mathbf{C}_{ih} \mathbf{T}_h := \mathbf{K}_{\mathbf{M}_{i,h}^{\Delta}} \mathbf{T}_h \tag{4}$$

and considering that $\tilde{\Phi}_i = \mathbf{C}_{ih}^T [\,\tilde{a}_i^1\ \tilde{a}_i^2\ \ldots\ \tilde{a}_i^F\,]^T$ with

$$\tilde{a}_i^{\tilde{e}} := \int_{\tilde{e},i} a^h(r) \cdot dl_i \tag{5}$$

which is defined as the integral of the magnetic vector potential along the dual edge $\tilde{e}$ of the grid of the ith subdomain; after substituting (3) in (5), we can express each $\tilde{a}_i^{\tilde{e}}$ generated by the currents $\mathbf{I}_h$ as

$$\tilde{a}_i^{\tilde{e}} = \sum_{n}^{V_q} \sum_{k=1}^{F_{v_h^n}} \frac{\mu_0 I_h^k \tilde{e}_h^k}{8\pi\,|vol_h^n|} \cdot \int_{\tilde{e},i} P_{g,n}(r) dl_i. \tag{6}$$

Here, V_q is the total number of volumes in Ω_h, whereas $F_{v_h^n}$ is the number of faces of a fixed v_h.

In conclusion, the previously introduced mutual constitutive matrix between two volumes $v_i \in \Omega_i$ and $v_h \in \Omega_h$ can be defined as

$$M_{ih}^{kn} = \frac{\mu_0 \tilde{e}_h^k}{8\pi\,|vol_h^n|} \cdot \int_{\tilde{e},i} P_{g,n}(r) dl_i. \tag{7}$$

Eventually, by separating the block matrices belonging to a self-subdomain from the ones linking two different subdomains, (1) can be reinterpreted as

$$\mathbf{K}_{SD}\mathbf{T} + j\omega\mathbf{K}_{\Delta}\mathbf{T} = \mathbf{b}_s \tag{8}$$

with

$$\mathbf{K}_{\Delta} = \begin{bmatrix} \mathbf{0} & \mathbf{K}_{\mathbf{M}_{1,2}^{\Delta}} & \cdots & \mathbf{K}_{\mathbf{M}_{1,N}^{\Delta}} \\ \mathbf{K}_{\mathbf{M}_{2,1}^{\Delta}} & \mathbf{0} & \cdots & \mathbf{K}_{\mathbf{M}_{2,N}^{\Delta}} \\ \vdots & \vdots & \ddots & \vdots \\ \mathbf{K}_{\mathbf{M}_{N,1}^{\Delta}} & \mathbf{K}_{\mathbf{M}_{N,2}^{\Delta}} & \cdots & \mathbf{0} \end{bmatrix}. \tag{9}$$

III. Iterative Method Comparison

Equation (8) can be used to derive different iteration schemes. As announced, in this section, we compare the GS scheme with the Krylov subspace schemes. Specifically, we will focus our attention on GMRES mainly, in addition to the conjugate gradient squared (CGS) method, the bi-conjugate gradient stabilized (BiCGSTAB) method, and the transpose-free quasi-minimal residual (TFQMR) method, whose descriptions can be found in [14]. As explained in [15], preconditioned conjugate gradient (PCG) cannot be applied, since the iteration matrix is not Hermitian or positive-definite, and thus, previously listed methods are the natural choice.

Furthermore, we specify that the mutual matrix $\mathbf{K}_{\Delta}$ could not be computed and stored in reality. In fact, for all the iterative algorithms here proposed, only the computation of $\tilde{\Phi}_{\Delta} = \mathbf{K}_{\Delta}\mathbf{T}$ is necessary as a result of the application of $\mathbf{K}_{\Delta}$ to a given $\mathbf{T}$. Thanks to this, required memory can be drastically reduced, since the matrix storage is limited to the only $\mathbf{K}_{SD}$, thus allowing to increase the problem-size dimensions both in terms of absolute geometrical dimension and in terms of

Authorized licensed use limited to: University of Udine. Downloaded on January 25,2021 at 10:42:39 UTC from IEEE Xplore. Restrictions apply.

DOF number. Surely, an efficient computation of $\tilde{\Phi}_\Delta$ is crucial for this approach to be competitive, and, indeed, in [16], it has been already shown that this can be done, since $\tilde{\Phi}_\Delta$ computation is massively parallelizable.

A. Gauss–Seidel

Applying the GS method means, at each step, finding one of the $\mathbf{T}_i \in \Omega_i$ of (8) by using the most recent $\mathbf{T}_j$, $j \neq i$ on the other subdomains to compute the contribution $\tilde{\Phi}_i = \mathbf{K}_\Delta(i,:)\mathbf{T}$ on that specific subdomain Ω_i, that is

$$\mathbf{K}_i \mathbf{T}_i^{n+1} = \mathbf{b}_{s,i} - j\omega\tilde{\Phi}_i^n. \tag{10}$$

The solution $\mathbf{T}_i$ is then updated to be available to find $\mathbf{T}_{i+1}^{n+1}$ in the next subdomain Ω_{i+1}. As explained before, $\tilde{\Phi}_i^n$ is evaluated on the fly thanks to (6).

B. Krylov Subspace Methods

The Krylov subspace methods allow to avoid finding a single $\mathbf{T}_i$ on a single Ω_i step by step, and they ensure convergence also when the inductive coupling between the subdomains is strong.

These algorithms just require a routine that can apply (8) to an arbitrary DOF vector $\mathbf{T}^*$ and compute the left-hand side value. The implemented routine performs the matrix-vector product $\mathbf{K}_{SD}\mathbf{T}^*$, and then, the additional contribution $\tilde{\Phi}_\Delta^* = \mathbf{K}_\Delta \mathbf{T}^*$ is calculated in the same fashion as previously described. In this case, one iteration corresponds to N GS sub-iterations, where N is the number of Ω_c partitions.

The efficiency of the Krylov subspace methods depends on the spectral properties of the matrix. In our setting, we choose to precondition the linear system with $\mathbf{P} = \mathbf{K}_{SD}^{-1}$. By this way, the computing cost between the GS and the other methods can be evenly compared, because, in both cases, the solution of the self-subdomains system $\mathbf{K}_{SD}\mathbf{T} = \mathbf{f}$ is necessary. The varying part is just related to the right-hand side $\mathbf{f}$.

C. Convergence Trend Comparison

Convergence tests reported in the following were done by using the boundary integral method, whose details are reported in [4]: this surface formulation is derived from the volumetric one previously described when written for triangular prisms with a constant thickness δ and yields to similar results as [5]. In Figs. 2 and 3, the geometries on which tests were done are shown. In particular, the comparison was carried out by using a first test case geometry constituted by three subdomains (3SD) and a second one with eight subdomains (8SD).

First of all, GS, CGS, BICGSTAB, TFQMR, and GMRES convergence trends have been compared on the same geometry. Results can be found in Fig. 4 for the 3SD geometry at $f = 10$ MHz; in this and in the following two graphs too, $\mathbf{T}_{\text{ref}}$ is the reference solution, whereas $\mathbf{T}_k$ is the solution after k function calls. Clearly, under this condition where the inductive coupling is strong, GMRES shows the best performance, whereas GS, CGS, and BICGSTAB have a similar behavior. On the other hand, due to the intrinsic higher function evaluation numbers of TFQMR and BCGSTAB (L) algorithms [14], their function call number is the greatest,

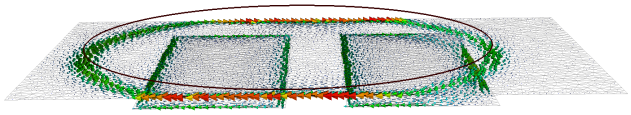

Fig. 2. Example of $re\{J\}$ distribution in the test case geometry with three distinct subdomains. Red circle represents the centerline of the magnetic field source coil. Major plate dimensions ($l \times w$): 20.0×13.2 mm^2.

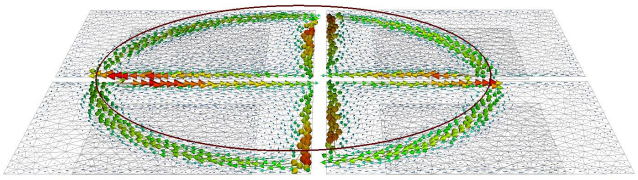

Fig. 3. Example of $re\{J\}$ distribution in the test case geometry with eight distinct subdomains. Red circle represents the centerline of the magnetic field source coil.

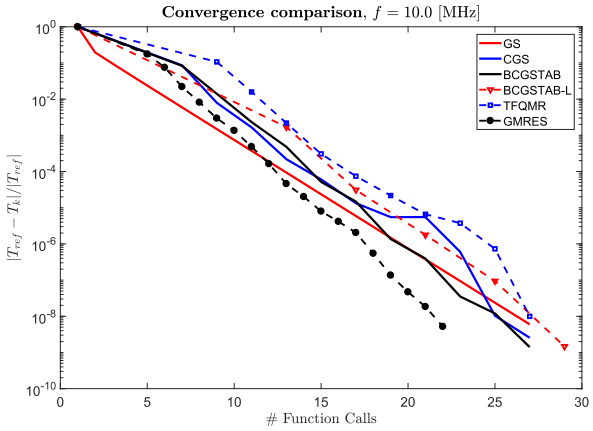

Fig. 4. Convergence trend comparison between GS, CGS, BICGSTAB, BICGSTAB (L), TFQMR, and GMRES at constant frequency and resistivity.

and so they will not be considered in the following part. The function call number represents the number of required computation of (8) to reach a given tolerance.

Figs. 5 and 6 compare GS and GMRES by varying the geometry size and the resistivity, respectively. In these plots, CGS and BICGSTAB results are not reported anymore, as their behavior is similar to GS. The same test was done by varying the frequency too, accomplishing similar results to Fig. 6.

As far as the geometry size variation is concerned, it is possible to state that there is not a significant variation of the maximum required iterations ($\text{IT}_{\max}$) when the geometry dimension increases. Differently, as already mentioned, when the inductive coupling of the problem increases, i.e., frequency becomes higher or resistivity reduces, an important $\text{IT}_{\max}$ variation occurs. Reasons of this behavior are well explained in Fig. 7, where the complex eigenvalues λ of the GMRES preconditioned iteration matrix (assembled only for the testing purposes) are showcased: when the frequency increases, λ values are moved away from the unity, thus increasing the spectral radius that adversely affects the convergence of the iterative methods. In this case, GS convergence slows down, and thus, using GMRES becomes an effective tool to limit the number of iterations.

Authorized licensed use limited to: University of Udine. Downloaded on January 25,2021 at 10:42:39 UTC from IEEE Xplore. Restrictions apply.

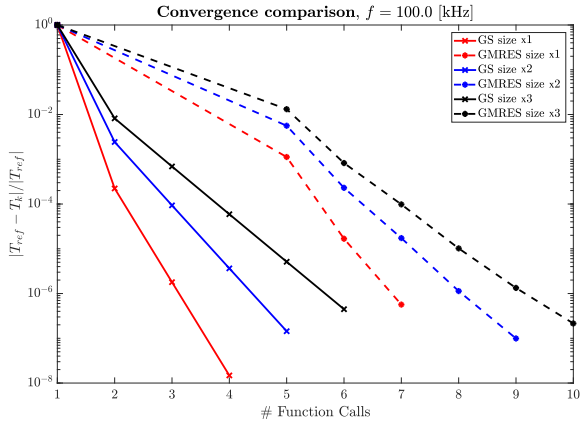

Fig. 5. Convergence trend comparison on the 3SD geometry between the GS and the GMRES with the increasing domain size. Mesh element size and plate thickness were kept constant, whereas l and w were multiplied by 2 ($x2$) and 3 ($x3$).

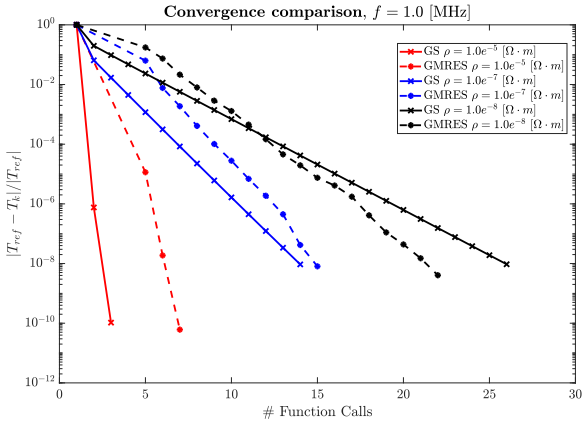

Fig. 6. Convergence trends comparison on the 3SD geometry between GS and GMRES with varying resistivities ρ. Other parameters were kept constant.

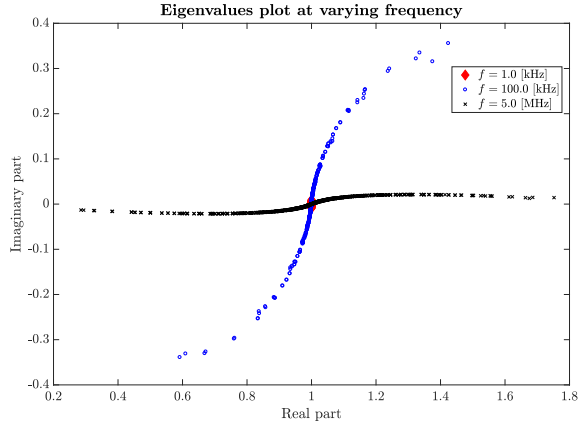

Fig. 7. Eigenvalues of the assembled equivalent system at varying frequencies.

Finally, regarding the number of partitions N, some tests have been performed on the *8SD* geometry in Fig. 3 by clustering the subdomains into different groups, thus obtaining three test geometries with two, four, and eight partitions. Results show that the iteration number does not change at all. The same behavior was observed when increasing the mesh density: the solution becomes more accurate, but $\mathrm{IT}_{\max}$ is practically constant. These two last tests show that the iterative scheme proposed is robust, and, differently to the one in [6], it can be used with an arbitrary geometry.

IV. Conclusion

In this article, a new direct-iterative hybrid scheme to solve the eddy currents on distinct subdomains by means of integral formulations was proposed. When a limitation in the memory occurs, this approach becomes convenient, since the most part of the matrix storage is avoided. Specifically, when the frequency is within some tens of kilohertz, the number of iterations is limited to a few iterations with both GS and GMRES methods. Conversely, when the frequency exceeds some megahertz and the resistivity is low like that one of a copper conductor, $\mathrm{IT}_{\max}$ becomes larger: in these cases, the GMRES scheme was shown to be effective to limit the required iterations and ensure convergence within some tens of iterations.

Acknowledgment

This work was supported in part by the Project Higher Education and Development (HEaD) Operation 1 University of Udine (UNIUD) of Friuli-Venezia Giulia Independent Region.

References

[1] S. Kurz, O. Rain, and S. Rjasanow, "The adaptive cross-approximation technique for the 3D boundary-element method," *IEEE Trans. Magn.*, vol. 38, no. 2, pp. 421–424, Mar. 2002.

[2] A. Kameari, "Transient eddy current analysis on thin conductors with arbitrary connections and shapes," *J. Comput. Phys.*, vol. 42, no. 1, pp. 124–140, Jul. 1981.

[3] R. Albanese and G. Rubinacci, "Integral formulation for 3D eddy-current computation using edge elements," *IEE Proc. A-Phys. Sci., Meas. Instrum., Manage. Educ.-Rev.*, vol. 135, no. 7, pp. 457–462, Sep. 1988.

[4] P. Bettini and R. Specogna, "A boundary integral method for computing eddy currents in thin conductors of arbitrary topology," *IEEE Trans. Magn.*, vol. 51, no. 3, Mar. 2015, Art. no. 7203904.

[5] P. Bettini, M. Passarotto, and R. Specogna, "A volume integral formulation for solving eddy current problems on polyhedral meshes," *IEEE Trans. Magn.*, vol. 53, no. 6, Jun. 2017, Art. no. 7204904.

[6] P. Bettini, M. Passarotto, and R. Specogna, "Iterative solution of eddy current problems on polyhedral meshes," *IEEE Trans. Magn.*, vol. 54, no. 3, Mar. 2018, Art. no. 7202304.

[7] I. D. Mayergoyz and G. Bedrosian, "Iterative solution of 3D eddy current problems," *IEEE Trans. Magn.*, vol. 29, no. 6, pp. 2335–2340, Nov. 1993.

[8] C. Geuzaine, A. Vion, R. Gaignaire, P. Dular, and R. V. Sabariego, "An amplitude finite element formulation for multiple-scattering by a collection of convex obstacles," *IEEE Trans. Magn.*, vol. 46, no. 8, pp. 2963–2966, Aug. 2010.

[9] Y. Saad and M. H. Schultz, "GMRES: A generalized minimal residual algorithm for solving nonsymmetric linear systems," *SIAM J. Sci. Stat. Comput.*, vol. 7, no. 3, pp. 856–869, 1986.

[10] A. Bossavit, "How weak is the 'weak solution' in finite element methods?" *IEEE Trans. Magn.*, vol. 34, no. 5, pp. 2429–2432, Sep. 1998.

[11] A. Bossavit, *Computational Electromagnetism: Variational Formulations, Complementarity, Edge Elements*. London, U.K.: Academic, 1998.

[12] G. Rubinacci and F. Villone, "The coupling surface method for the solution of magnetoquasi-static problems," *IEEE Trans. Magn.*, vol. 52, no. 3, Mar. 2016, Art. no. 7202804.

[13] M. Fabbri, "Magnetic flux density and vector potential of uniform polyhedral sources," *IEEE Trans. Magn.*, vol. 44, no. 1, pp. 32–36, Jan. 2008.

[14] Y. Saad, *Iterative Methods for Sparse Linear Systems*, 2nd ed. Philadelphia, PA, USA: SIAM, 2003.

[15] P. Joly and G. Meurant, "Complex conjugate gradient methods," *Numer. Algorithms*, vol. 4, no. 3, pp. 379–406, 1993.

[16] T. Maceina, P. Bettini, G. Manduchi, and M. Passarotto, "Fast and efficient algorithms for computational electromagnetics on GPU architecture," *IEEE Trans. Nucl. Sci.*, vol. 64, no. 7, Jul. 2017.

Authorized licensed use limited to: University of Udine. Downloaded on January 25,2021 at 10:42:39 UTC from IEEE Xplore. Restrictions apply.